Human stability during floods: Experimental tests on a physical model simulating human body

Human stability during floods: experimental tests on a physical model simulating human body

Matteo Postacchini[a], Gabriele Bernardini[a], Marco D'Orazio[a], Enrico Quagliarini[a,*]

[a]*Department of ICEA, Università Politecnica delle Marche, Ancona, Italy*

Abstract

Urban floods are becoming more and more intense and frequent allover the world. Extreme events are the main triggering factors of such floods, and merit attention for what concerns the urban planning and emergency strategies. Numerical models aimed at investigating the optimal paths for evacuees escaping a flooded urban environment may be used by local authorities to properly understand how to improve people safety and mitigate the flood risk. Implementation of empirical laws in such models to describe the people stability in flooded areas is thus crucial to understand the behavior of evacuees and rescuers during emergency conditions. Laboratory experiments have been undertaken using a physical model representing a human body at quasi-natural scale, towed by an electrical engine in the water at rest. This represents a novel laboratory approach which exploits a non-inertial reference frame in motion with the model. The experimental results, obtained using different combinations of water depth and flow speed, have led to empirical laws which outline the stability conditions occurring when either the model front or the model back faces the flow, these respectively corresponding to Backward Toppling Instability (BTI) and Forward Toppling Instability (FTI). Such laws have been found through comparison with reference literature works, using various statistical methods. The FTI condition has been seen to largely improve the human stability compared to BTI, in contrast to the results of previous literature works, which stated an overall similarity between the results of the two toppling conditions. To better understand the role of the water flow during the different tests, hydraulic forces and moments have been measured. It has been seen that dynamic and static effects are comparable during high-speed conditions, especially due to a relevant fluid-model interaction and an increase of the water-surface level, while dynamic effects are negligible during low-speed conditions. The results of the present contribution can represent an important step forward for the numerical models applied to the framework of urban and emergency planning.

Keywords: urban floods, laboratory experiments, human body stability,

*Corresponding author
Email address: e.quagliarini@staff.univpm.it (Enrico Quagliarini)

toppling, empirical laws

1. Introduction

In the recent years, the flood phenomenon has become significantly important due to a larger negative impact on both people and environment. Many are the factors affecting such phenomenon and its rate of change. Among others, climate change is one of the main drivers, which characterizes the worldwide climate, e.g. leading to a gradual temperature increase (Kundzewicz et al., 2014). Climate changes have a large impact on the hydrological cycle, as confirmed by many recent studies (e.g., Huntington, 2006; Pachauri et al., 2014), with the human factor playing a major role, e.g., for what concerns the flow regime (Brown et al., 2005; Ma et al., 2008; Memmola and Darvini, 2018; Darvini and Memmola, 2020).

Although heavy precipitations are one of the main causes of river floods (see the data published by the Dartmouth Flood Observatory[1]), rainfalls cannot be easily ascribed to a clear trend, like the increase of precipitation intensity with time. These seem to rely more on local factors, like orography, than on climate change (Soldini and Darvini, 2017). Further, the change in river runoff is significantly related to both climate change and human activity (Memmola and Darvini, 2018; Darvini and Memmola, 2020), though the interconnection between such factors cannot be easily neglected (Zhang et al., 2001; Wang et al., 2013).

Among the weather-related disasters, in the period 1995-2015, floods were the most frequent and affected the highest number of people globally, with about $157,000$ deaths and economic losses of about US$ 662 billion (CRED, 2015). Hence, floods are among the major natural disasters which typically occur allover the world, and important solutions are thus required, e.g. aiming at smart cities which are sufficiently resilient to urban floods (Fang, 2016).

However, due to the scarcity of field data in urban environments during floods (Brown and Chanson, 2012; Chanson et al., 2014), numerical simulations of such events is fundamental to provide useful information to managers, authorities, as well as to everyone dealing with urban floods and following emergency state (Dottori et al., 2013; Mignot et al., 2019). Such simulations need to be set up starting from robust data sets, e.g. suitable topographies or hydrodynamic boundary conditions, rather than on very high-resolution schemes (Dottori et al., 2013). Meanwhile, suitable relations between floodwater conditions and the individuals' response in terms of behaviors and motion features are crucial to perform meaningful evacuation simulations.

Recent research efforts led to the coupling of hydraulic models, for the description of floodwater features, and behavioral models, for the description of evacuees' motion in emergency conditions. It has been seen that the combined

[1] Website: http://floodobservatory.colorado.edu/index.html. Last access: 02/03/2020

use of such models aimed at describing flood-induced evacuation, represents a suitable solution and can provide an important aid to the involved stakeholders (Bernardini et al., 2017; Kim et al., 2018; Mollah et al., 2018). Such approach is particularly important when specific conditions occur, e.g. when warning systems are not available within the urban area or when the flood phenomenon is relatively rapid (e.g. due to levee failure in proximity of the urban area). In this conditions, the above-mentioned models may help to develop suitable strategies (e.g., signs, architectural elements to be applied in the riskiest areas), which are fundamental for driving people toward safe areas during their evacuation.

With the aim to better understand how floodwaters impact the people safety, full scale laboratory experiments were recently conducted to determine the motion speed of evacuees while moving in floodwaters, by providing consolidated bases to model such aspect (Bernardini et al., 2020). Efforts in determining the human stability laws have also been evaluated through analytical solutions and experimental tests. Real-scale tests have been also performed to evaluate the effects of floodwater forces on human actions exerted during the evacuation (Baba et al., 2017).

The study of the forces involved in the equilibrium of a human body partially immersed and subject to a water flow concerns two instability mechanisms (Xia et al., 2014):

- the *sliding* mechanism, related to the equilibrium along the horizontal plane over which the body is standing,
- the *toppling* mechanism, related to the moment equilibrium around a pivot, i.e. typically the foot heels.

In both mechanisms, the instability contribution is related to the drag force exerted by the flow. While the resisting contributions are represented by the friction force and the moment provided by the gravity force, respectively in the sliding and toppling mechanisms. In addition, the buoyancy force plays a negative role in the moment balance, hence reducing the stabilizing contribution of the body weight in the toppling mechanism.

Some recent works investigated the human body stability under floodwater conditions related to the above mechanisms (Xia et al., 2014). Experiments have been carried out using volunteers (Foster and Cox, 1973; Abt et al., 1989; Jonkman and Penning-Rowsell, 2008; Shand et al., 2011) rather than models, which can be of different nature, i.e. either analytical, numerical or physical models (Cox et al., 2010; Xia et al., 2014; Milanesi et al., 2015; Arrighi et al., 2017, 2019). Results of such approaches provide critical curves describing the human body stability condition. Numerical simulators for the modeling of the pedestrian evacuation during floods require a suitable description of such critical conditions, in terms of water depth and flow speed.

The presented work provides further results on the floodwater critical conditions, which are functions of water depth and flow speed by means of a dummy at a quasi-natural scale, hence much larger than typical laboratory experiments

used for retrieving the classical critical curves (e.g., Xia et al., 2014). In addition, the present experiments provide precautionary and objective results if compared to the experiments with volunteers (e.g., Foster and Cox, 1973), which are quite hard to be reproduced in completely safe conditions. A further novel aspect concerns the model set up, i.e. results have been here obtained using the dummy either facing the flow or with the back toward the flow. Such a double set up has been rarely tested, and literature works state that both flow/dummy orientations lead to almost the same instability results (e.g., Xia et al., 2014). Conversely, important differences have been observed in our experiments, as shown in the following sections.

The manuscript is divided as follows. Section 2 describes the laboratory experiments, whose elaborations are reported in section 3. Section 4 provides an overall discussion of the results, also in relation to future implementation of results in modeling approaches, while section 5 outlines the final conclusions.

2. Materials and Methods

The approach used in the present follows specific phases as detailed below:

1. definition and construction of the physical model (dummy) to be used in the laboratory tests,
2. instability tests with different water depths and flow speeds with the model facing the flow, also called Forward Toppling Instability (hereafter FTI),
3. instability tests with different water depths and flow speeds with the model back toward the flow, also called Backward Toppling Instability (hereafter BTI),
4. fixed-model tests with different water depths and flow speeds, aimed at measuring water pressures at different levels,
5. definition of the limit stability regression curves for BTI and FTI,
6. analysis of hydrodynamic forces and moments at the different flow conditions.

Concerning points 2, 3 and 4, the experimental tests were carried out in the Laboratory of Hydraulics and Maritime Constructions of the Università Politecnica delle Marche (Ancona, Italy), previously used in floodwater-man interactions experiments (Bernardini et al., 2020). A wave flume, commonly aimed at hosting maritime physical models, was used for the present campaign. The channel (Figure 1) is $50m$ long, 1.3 deep and $1m$ wide. Steel uprights and glass walls characterize the whole flume length, while the bottom over which the tests were carried out is made of concrete mortar.

2.1. Physical model and baseline setup

The scope was that of mimicking the fluid-solid interaction occurring when an individual is subject to floodwater conditions. For safety reasons and to reach feasible results, a large physical model similar to a dummy was thus reproduced.

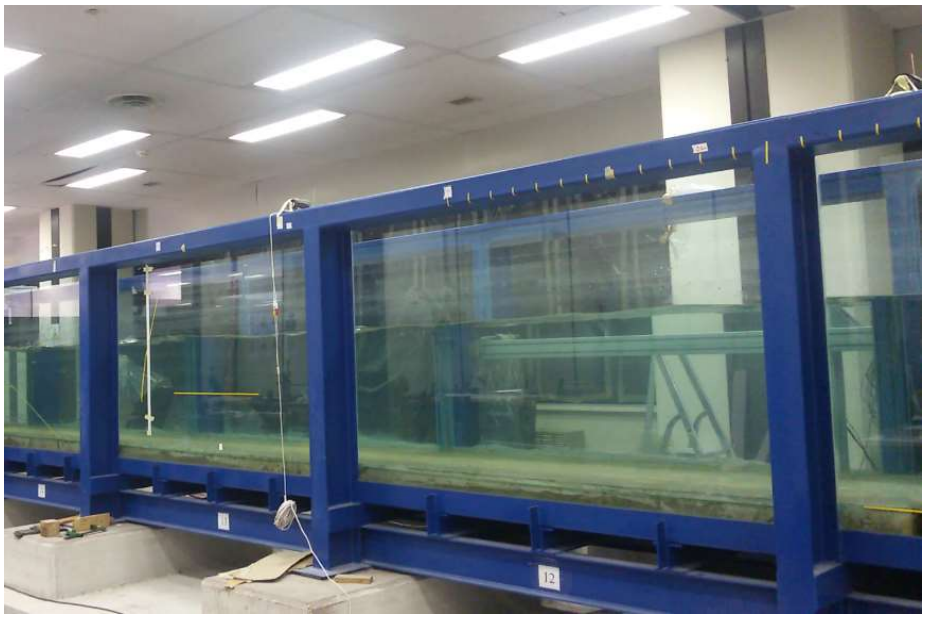

Figure 1: Wave flume where experiments were carried out.

Following Lind et al. (2004) and Milanesi et al. (2015), a simplified model was realized to properly reproduce the involved forces and moments. Considering an individual of height H, such approach suggests the use of a cylinder of diameter D and height $H/2$ to represent the upper part of the human body, while two cylinders of diameter $D/2$ and height $H/2$ reproduce the lower part. Two thin sheets represent the feet.

Hence, inspired by such approach, a dummy has been reproduced at a reduced scale (1 : 1.6) and then used for the experimental campaign here presented. Since the ratio between model and prototype lengths, i.e. the length scale, is $\lambda_l = 1/1.6 = 0.625$, the Froude similarity, typically used in experiments where inertial and gravity forces are the dominating contributions (e.g., see Heller, 2011), suggests a velocity scale $\lambda_v = \lambda_l^{1/2} = 0.791$. Similarly, volume, mass and force scales with $\lambda_V = \lambda_m = \lambda_F = \lambda_l^3 = 0.244$, while the pressure scale is equal to the length scale $\lambda_p = \lambda_l = 0.625$.

Starting from the anthropometric study by Webb Associates (1978) and based on the anthropometric analysis of volunteers enrolled to evaluate the human motion in floodwater conditions (Bernardini et al., 2020), a male individual at prototype scale with height of $H_P = 180cm$ and mass of $m_P = 80kg$ was selected for the present laboratory experiments. To this aim, three rigid PVC cylinders were used (see Figure 2), one for the upper part of the body, two for the lower part. In addition, to properly reproduce the toppling motion, the feet were also modeled by using two separate PVC plates connected to the lower cylinders. Such plates were $16cm$ long, $10cm$ wide and $1cm$ thick.

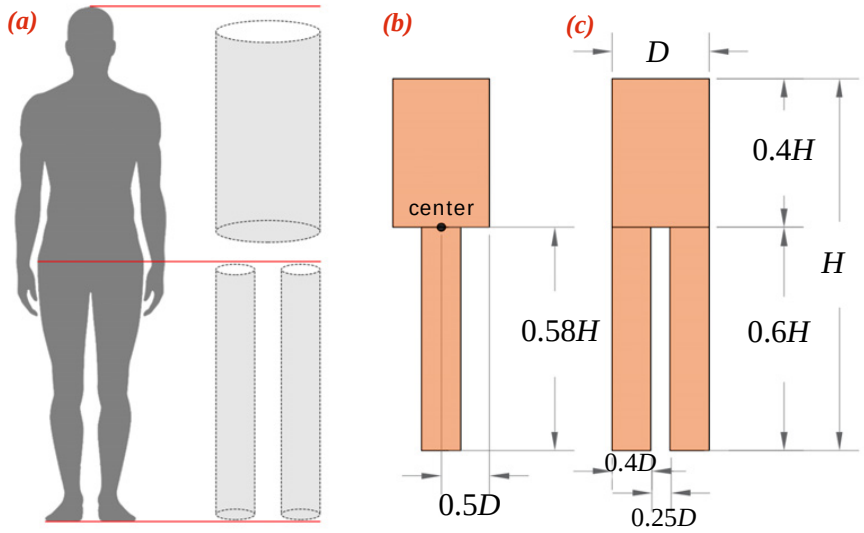

Figure 2: Sketch of the reproduced physical model: (a) dummy concept (frontal view), (b) location of the center of mass (side view), (c) main geometrical characteristics (frontal view). All dimensions depend on either D or H.

Following the above-mentioned indications, the dummy at reduced scale was made as follows. Provided that the total height of the model was required to be $H_M = \lambda_l H_P = 112.5cm$, the upper and lower parts were chosen to be as close as possible to, respectively, $0.4H_M$ and $0.6H_M$. In particular, the single cylinders, i.e. without considering the connections between them and the foot thickness, were characterized by a height of $43cm$ (upper cylinder) and $60cm$ (lower cylinder). Further, the upper cylinder was characterized by a diameter $D_M = 25cm$ and the lower cylinders by a diameter $0.4D_M = 10cm$. Every cylinder was filled with a mixture of sand and foam rubber, so as to obtain a total mass of the model $m_M = 19.57kg \approx \lambda_m m_P$. Under this perspective, the total volume was $V_M = 25.38dm^3$ and the mean density $\rho_M \cong 770kg/m^3$. The center of mass of the single cylinders was properly adjusted, so as to have the center of mass of the human body in agreement with Milanesi et al. (2015)'s indications. The center of mass coordinates were thus $(x_c, y_c) = (0.5D, 0.58H)$ (Figure 2).

The upper cylinder was properly sealed on the top. Upper and lower cylinders were linked through use of caps, which were pierced and connected by means of bolts. Lower cylinders and feet were linked using glue and screws. The sizes used for the construction of the physical model have been reported in Table 1, where the starting point, i.e. the real-world prototype, is also described (Herman, 2016).

To evaluate the toppling stability in the presence of different floodwater conditions, the feet of the constructed model were hinged on the top plate of a trolley. In fact, for the present experiments, the effect of the flow impacting

Table 1: Details of both real prototype and scaled physical model. Notice that length refers to the larger dimension. The smaller prototype dimension is either the thickness (for foot) or width (for upper and lower parts), this corresponding to the diameter D at model scale.
† Ankle to bottom of foot

Piece	#	**main size**		**secondary size**		**mass**	
		prototype [cm]	*model* [cm]	*prototype* [cm]	*model* [cm]	*prototype* [kg]	*model* [kg]
upper part	1	68.94	43.00	39.60	24.75	49.44	12.07
lower part	2	95.40	60.00	15.68	9.80	14.34	3.50
foot	2	27.36	17.10	7.02†	1.00	1.01	0.25

the human body was obtained by moving such trolley in the water at rest and assuming a non-inertial reference frame in motion with the trolley. A mechanical system, made of an electrical engine connected to the trolley by means of four pulleys and a toothed belt, allowed the model to move along a free-from-obstacle length of about $16m$ (further details are provided in Postacchini et al., 2019). The above described experimental setup, including the physical model, are illustrated in Figure 3.

To improve the measurement accuracy and check the correspondence between engine rotation and trolley motion, the speed of the human body in the water at rest was measured using two methods, i.e. (1) a couple of photocells placed $2m$ far apart, measuring the speed of the human body, and (2) the inverter, measuring the engine rotations. No relevant measurement differences have been observed between such methods.

2.2. Pressure measurements

An additional configuration, characterized by the human body in fixed position during the whole trolley motion, i.e. with no possibility to topple, was tested to measure the pressure field and with the aim to evaluate the forcing action of the flow during stability and instability conditions. For this purpose, eight Piezoresistive Pressure Transmitters (Keller - Series 23SY and 25Y) were deployed along the model legs, specifically four sensors each, to better exploit the available space and assuming the flow as symmetrical with respect to the vertical plane passing through the model center of mass. Figure 4 and Table 2 illustrates location and distance from the bottom surface of such sensors.

2.3. Test methodology

The experimental tests were carried out exploiting a non-inertial reference frame. To this aim, the trolley over which the human body was standing, was initially at rest. It started moving and accelerated, then moved in the flume for about $16m$, finally it decelerated and stopped (details can be found in Postacchini et al., 2019). To prevent the body instability during the acceleration phase, a little hook was used to maintain the body standing. After the acceleration

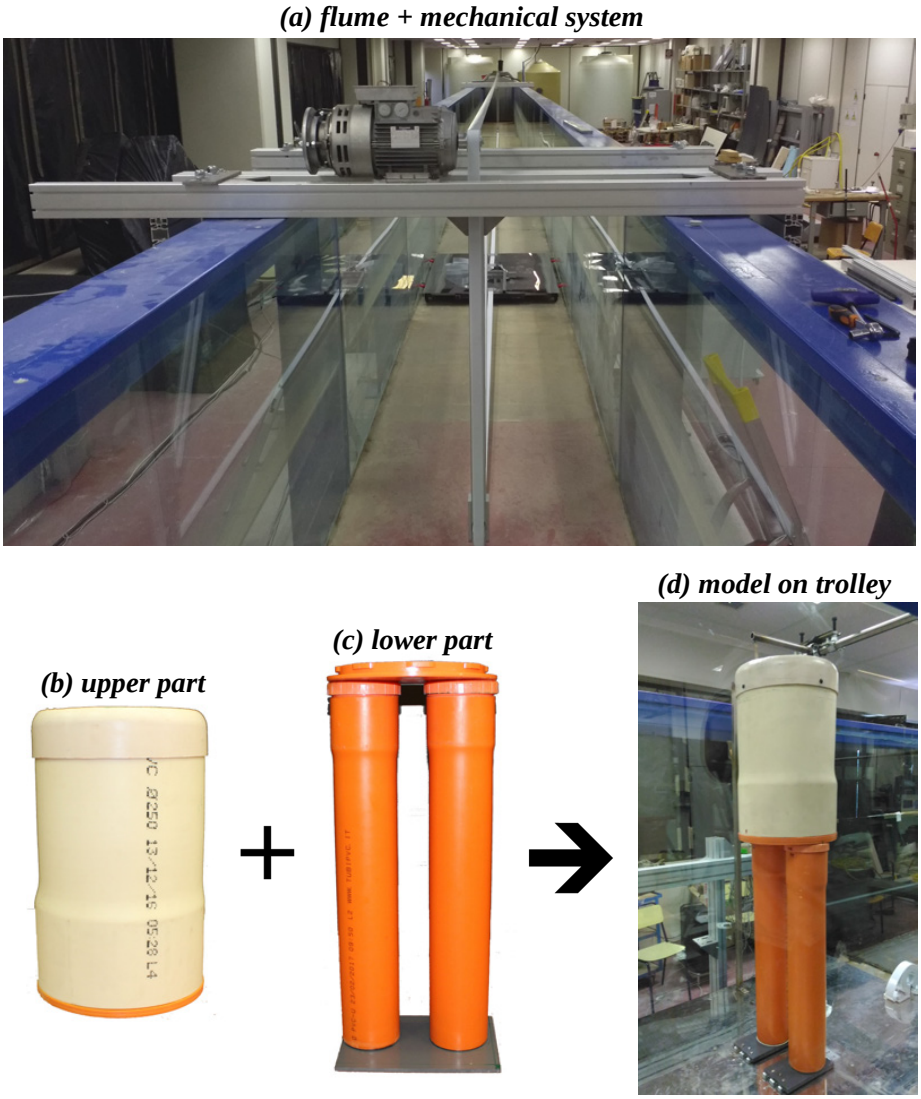

Figure 3: Pictures representing: (a) the flume and the mechanical system (engine, pulleys, toothed belt and trolley); (b) upper and (c) lower parts of the physical model; (d) complete model standing on the trolley in the flume.

phase, the hook was released to allow the body to topple in the case critical conditions occurred.

Two different positions of the human body were tested, to analyze the instability conditions when the body was hinged in correspondence of either heel (backward toppling, see Video 1 under Supplementary Material) or toe (forward toppling, see Video 2 under Supplementary Material). The expected differences

Figure 4: Sensor location along the model legs.

sensor-bottom distance *prototype* [cm]	*model* [cm]	leg	series
9.8	6.1	L	25Y
18.1	11.3	R	25Y
25.6	16.0	L	25Y
35.4	22.1	R	25Y
45.3	28.3	L	23SY
60.2	37.6	R	23SY
72.5	45.3	L	23SY
88.2	55.2	R	23SY

Table 2: Sensor distances from the bottom. **L** and **R** indicates left and right legs, respectively.

in the stability results concern the distance between the center of mass and the rotation point, which is larger in the case of forward toppling.

For both standing positions of the body, a fixed number of water depths was tested, combined with a variable number of the trolley speed, depending on the model equilibrium response. In detail, 14 water depths were tested, spanning in the range $h = (10-75)cm$, corresponding to $(16-120)cm$ at prototype scale. The tested speeds were in the range $V = (0.3-2.4)m/s$, corresponding to the real-scale speeds (0.4–3.0)m/s. Each combination have been tested at least five times for the sake of repeatability. Figure 5 shows the $h-V$ combinations used in the flume experiments (full yellow circles), which partially cover the typical curves referring to the pedestrians' stability conditions (here properly scaled to agree with the laboratory tests). In particular, 14 distinct water depths h were tested, each value associated to a series of speeds V, depending on the model stability. Tests with large depth values (symbols in the upper part of Figure 5) were characterized by a clear behavior, i.e. all repetitions of each $(h-V)$ test substantially provided the same response (either stability or toppling), while much more $(h-V)$ combinations were required with small depth values (lower part of Figure 5), due to the uncertain model behavior. Specifically, an unclear feedback was observed for test sequences with small h, i.e. among the five repetitions of each $(h-V)$ combination, at least one resulted in the model toppling, at least one in the model stability. Such unclear situations are marked as "uncertain" in the result section. With the purpose to draw critical curves for both BTI and FTI tests, at each investigated depth h the following points are used: i) the largest speed featuring a stable condition, ii) the smallest speed featuring an unstable condition, iii) the uncertain cases. Based on such critical points and with the aim to investigate forces and moments around the BTI curve, pressures were only measured for some $h-V$ combinations (empty blue circles in Figure 5) during the additional configuration, here sensorized tests,

described in Section 2.2.

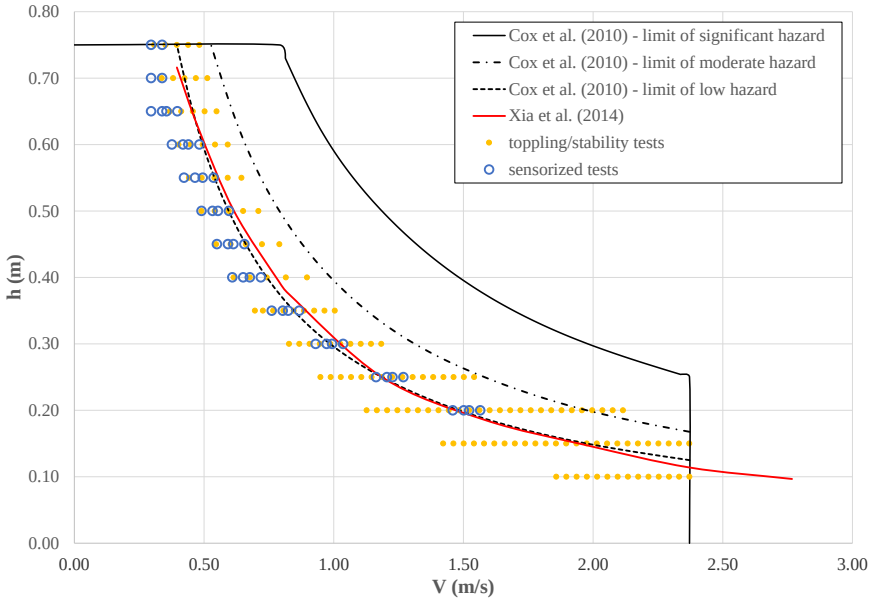

Figure 5: $h-V$ experimental pairs referring to the toppling/stability tests (full yellow circles) and to the sensorized tests (empty blue circles). Reference literature curves are also shown. h and V are expressed in the model scale.

About the literature curves, the black lines bound the regions where low (below dashed line), moderate (area between dashed and dash-dotted lines), significant (area between dash-dotted and solid lines) and extreme (area over solid line) hazard conditions exist for adults (Cox et al., 2010). Further, Xia et al. (2014)'s results are shown through the interpolating red curve, which is significantly close to (Cox et al., 2010)'s low hazard curve.

2.4. Regression modeling and comparison with literature works

Different regression models have been tested in such $V-h$ pairs, by considering V as the independent variable and h as the dependent variable, in agreement with the literature general trends shown by Figure 5. According to (Cox et al., 2010; Xia et al., 2014; Milanesi et al., 2015), the following models are proposed:

1. a power-based law, defined as $h = aV^b$,
2. a polynomial, 3rd-degree-based law,
3. a logarithm-based law, defined as $h = a + b\ log(V)$;
4. an exponential-based law, defined as $h = a\ exp(bV) + c$.

The coefficient of determination R^2 is calculated for each model. The regression models are considered valid within experimental pairs range, although their general trends outside of this border are additionally examined to estimate if

predictions can be ideally extended within the V and h ranges of reference models (Cox et al., 2010; Xia et al., 2014; Milanesi et al., 2015). Each tested model has been compared to the literature models according to the methodologies already used for the analysis of the for man-floodwater interaction (e.g., see Bernardini et al., 2020).

First, the Secant Cosine, SC [−] (Ronchi et al., 2013), is calculated to evaluate the shape similarity between h_{exp} (h estimation related to one of the proposed regression models) and h_{ref} (water level referring to the considered reference studies). To evaluate the adherence to the existing literature models (Cox et al., 2010; Xia et al., 2014; Milanesi et al., 2015), this study assumes that the selected model with the best combination between R^2 and $\overline{SC}$ values for both FTI and BTI conditions will be assumed as the most representative of the experimental test results.

Then, the related position of the curves is assessed according to the following methods. The "Difference between the graphic Areas Under the Curves" ($DAUC$ [%]) method allows evaluating the difference of predicted h values within the experimental V range. DAUC is calculated according to the following equation:

$$DAUC = \frac{\int_{V_{min}}^{V_{max}} h_{exp} dV - \int_{V_{min}}^{V_{max}} h_{ref} dV}{\int_{V_{min}}^{V_{max}} h_{exp} dV} \ [\%], \tag{1}$$

where V_{min} and V_{max} are the experimental limits of the tested V range. Each integral thus represents the area below a specific curve, which may also be graphically estimated. Such method traces how much the proposed curves differ from those related to the reference works. Specifically, positive $DAUC$ values mean that the proposed models provide water levels higher than those coming from the the reference models: in such cases, the toppling conditions are related to "riskier" values compared to the reference-model values. The "Euclidean Projection Coefficient", EPC [−] (Ronchi et al., 2013), has been calculated to define the "factor which, when multiplied by each data point" of the regression model h_{exp}, reduces the distance between the estimated h_{exp} and h_{ref}.

Finally, the best model is compared to the pressure measurements with the aim to highlight the specific phenomena involving the body stability also in comparison to the literature modeling. Specifically, the triangular pressure distribution that characterizes the flow at rest before the beginning of each test, i.e. a zero pressure at the water surface and a maximum pressure at the bottom ($p_{st} = \gamma h$), has been used to calculate the hydrostatic force (F_{st}). On the other hand, during the dummy motion, a dynamic pressure p_d generates, this strongly depending on the V value, and has been used to calculate the hydrodynamic force (F_{dyn}), as previously done in (Postacchini et al., 2019). Both forces have been evaluated for each test, i.e. for each $h-V$ pair, this providing the total force ($F_{tot} = F_{st} + F_{dyn}$) exerted on the dummy. With the aim to understand the human instability, the overturning moments generated by all hydraulic forces have been estimated, i.e. both static (M_{st}), dynamic (M_{dyn}) and total (M_{tot}) moments.

Both forces and moments have been obtained in the following way: the static contributions have been evaluated in a wide $h - V$ region using the hydrostatic law, while the dynamic contributions have been obtained using a biharmonic spline interpolation[2] of the recorded data. The sum of static and dynamic contributions has led to the total contributions. Such results are illustrated using color maps, with the value of each component being represented by a specific color tone. This enables one representing the results on the $h - V$ plane. The best previously defined regression models (one referring to BTI, one to FTI) have been overlapped to such color map, with the aim to evidence the trend of the forces with respect to the regression model, e.g. in respect to toppling and sliding phenomena evidenced by the literature works (Cox et al., 2010; Xia et al., 2014; Milanesi et al., 2015).

2.5. Analysis of dimensionless mobility parameters

To better understand both BTI and FTI behaviors with respect to the recent literature (Arrighi et al., 2017, 2019), the data used for the regression curves (as described in section 2.4) are also investigated using dimensionless numbers. In these terms, the flow characteristics h and V are summarized by the Froude number:

$$Fr = \frac{V}{\sqrt{g\overline{h}}} \tag{2}$$

where g is the gravity acceleration. The fluid-body interaction is described by both relative height $\overline{h}$ and mobility parameter for toppling and sliding instability θ_P, defined as follows:

$$\overline{h} = \frac{h}{H_P} \tag{3}$$

$$\theta_P = \frac{2d_f}{H_p}\frac{H_P - h}{h} \tag{4}$$

where the person height is $H_P = 1.80m$ and the foot length $d_f = 0.27m$ in the present tests, both values at prototype scale.

BTI and FTI data series used for the regression curves are here used to compare with the existing literature and to try to explain the role of both sliding and toppling mechanisms.

3. Results

3.1. Stability analysis

The results from all tests, converted into prototype scale, are illustrated in Figure 6.

[2]The 2-D interpolation, which is not triangulation-based, is part of the MATLAB function "*griddata*". Web manual: `https://www.mathworks.com/help/matlab/ref/griddata.html`

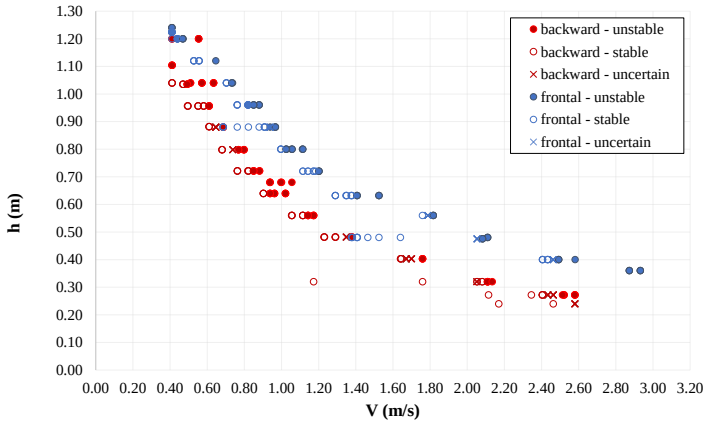

Figure 6: Results of both BTI (red symbols) and FTI (blue symbols) tests: unstable condition (•), stable condition (○) and uncertain condition (×). Prototype scale.

In details, the BTI results were obtained hinging the model on the heels, which represents the classical analyzed standing, due to a smaller stabilizing moment due to a smaller distance to the application point of the body weight (see Video 1 under Supplementary Material). Conversely, the FTI results were obtained hinging the model on the foot toe (see Video 2 under Supplementary Material). This provided a larger stabilizing moment due to a larger distance between the hinging location and the application point of the body weight.

The comparison among such results clearly shows the wide difference in the stability provided by the two model configurations, especially for relatively small water depths and relatively fast flows. As an example, a speed $V = 2.6m/s$ provides critical conditions during the BTI configuration when the water depth is $h = 0.27m$, while the FTI configuration is associated to a critical depth $h = 0.40m$. In other words, people subject to a relatively fast flow coming from the front rather than from the back largely improve the human stability, with an increase of the critical water depth of more than 40%. Conversely, relatively large depths are associated to critical speeds which are comparable for the two configurations, e.g. a water depth $h = 1.20m$ leads to instability when $V = 0.41m/s$ and $0.44m/s$ in the case of, respectively, BTI and FTI configurations. This means an increase of critical speed of less than 10%.

3.2. Regression modeling

The regression model results for BTI and for FTI are respectively shown by Table 3 and Table 4, where the model form, parameters and statistical values estimated with respect to the the reference literature models, i.e. R^2 and $\overline{SC}$ (representing mean SC values), are shown. Table 5 summarizes SC, EPC and $DAUC$ with respect to each literature model for both BTI and FTI data series.

Finally, Table 6 provides an overview of the model validity outside of the range of experimental pairs, in comparison to the main aspects of the literature works.

Table 3: BTI regression model analysis.

Model	Equation	Model parameters				R^2	$\overline{SC}$
		a	b	c	d		
expon.	$h = a\ e^{bV} + c$	1.63	-1.37	0.22	-	0.995	0.990
log.	$h = a + b\ log(V)$	0.66	-0.48	-	-	0.981	0.964
poly.	$h = aV^3 + bV^2 + cV + d$	-0.15	0.90	-1.90	1.78	0.995	0.979
pow.	$h = a\ V^b$	0.60	-0.78	-	-	0.984	0.987

Table 4: FTI regression model analysis.

Model	Equation	Model parameters				R^2	$\overline{SC}$
		a	b	c	d		
expon.	$h = a\ e^{bV} + c$	1.43	-0.88	0.24	-	0.995	0.980
log.	$h = a + b\ log(V)$	0.83	-0.48	-	-	0.989	0.966
poly.	$h = aV^3 + bV^2 + cV + d$	-0.04	0.35	-1.11	1.64	0.996	0.981
pow.	$h = a\ V^b$	0.79	-0.57	-	-	0.961	0.987

Table 5: BTI and FTI regression model comparison with the reference works.

	SC / EPC [-] (DAUC [%])				
Model	Cox et al. (2010)			Xia et al. (2014)	Milanesi et al. (2015)
	significant hazard	moderate hazard	low hazard		
BTI expon.	1.00 / 0.53 (-46)	0.99 / 0.77 (-21)	0.98 / 0.96 (3)	1.00 / 0.96 (1)	0.99 / 0.72 (-31)
BTI log.	0.97 / 0.53 (-44)	0.95 / 0.77 (-18)	0.94 / 0.96 (5)	0.97 / 0.96 (3)	0.99 / 0.72 (-30)
BTI poly.	0.97 / 0.54 (-45)	0.98 / 0.77 (-20)	0.97 / 0.96 (4)	0.99 / 0.96 (2)	0.98 / 0.72 (-30)
BTI pow.	1.00 / 0.54 (-44)	1.00 / 0.76 (-19)	1.00 / 0.96 (4)	1.00 / 0.96 (2)	0.94 / 0.73 (-30)
FTI expon.	0.99 / 0.76 (-21)	0.96 / 1.03 (12)	0.99 / 0.76 (42)	0.97 / 1.23 (40)	1.00 / 0.91 (-7)
FTI log.	0.96 / 0.76 (-21)	0.95 / 1.03 (12)	0.96 / 0.76 (42)	0.97 / 1.23 (40)	0.99 / 0.91 (-7)
FTI poly.	0.99 / 0.76 (-21)	0.96 / 1.03 (12)	0.99 / 0.76 (42)	0.97 / 1.23 (40)	1.00 / 0.91 (-7)
FTI pow.	0.99 / 0.78 (-17)	0.99 / 1.02 (15)	0.99 / 0.78 (45)	1.00 / 1.23 (43)	0.97 / 0.92 (-5)

According to Table 5, all the proposed regression models for BTI and FTI have a similar trend compared to the literature models, in terms of curve shape (according to the SC values, always > 0.94), EPC values and DAUC values. Specifically, DAUC and EPC values evidence how:

1. the BTI-related proposed models are generally similar to Cox et al. (2010)'s curve for the limit of low hazard and Xia et al. (2014)'s curve (e.g. compare to Figure 7 for the exponential curve), thus representing the most critical conditions for human stability;
2. the FTI-related proposed models are generally placed over Cox et al. (2010)'s curve for the limit of low and moderate hazard and Xia et al.

Table 6: Analysis of BTI and FTI regression model outside of the experimental pairs range and comparison with the main reference works issues.

Model	h for $V = 0m/s$ [m] FTI	BTI	Notes	V for $h = 0m$ [m/s] FTI	BTI	Notes
expon.	1.67	1.85	limits consistent with Milanesi et al. (2015) for adult toppling ($1.71m$), max abs. error: 7%	horizontal asymptote at $h = 0.24m$	horizontal asymptote at $h = 0.22m$	upper limit in V should exist due to sliding (e.g. $V = 3m/s$ Cox et al., 2010)
log.	$+\infty$	$+\infty$	upper limit in h due to buoyancy should exist (e.g. $h = 1.2m$ Cox et al. (2010))	5.63	3.96	BTI limit is comparable with sliding limit in Cox et al. (2010)
poly.	1.64	1.78	limits consistent with Milanesi et al. (2015) for adult toppling ($h = 1.71m$), max abs. error: 4%	4.70	3.20	the BTI limit is consistent with Cox et al. (2010)
pow.	$+\infty$	$+\infty$	upper limit in h due to buoyancy should exist (e.g. $h = 1.2m$ Cox et al. (2010))	$+\infty$	$+\infty$	upper limit in V should exist due to sliding (e.g. $V = 3m/s$ Cox et al., 2010)

(2014)'s curve (e.g. compare Figure 8 for the exponential curve), thus predicting less risky conditions in terms of $V - h$ pairs compared to such literature laws ($DAUC > 0$, $EPC > 1$).

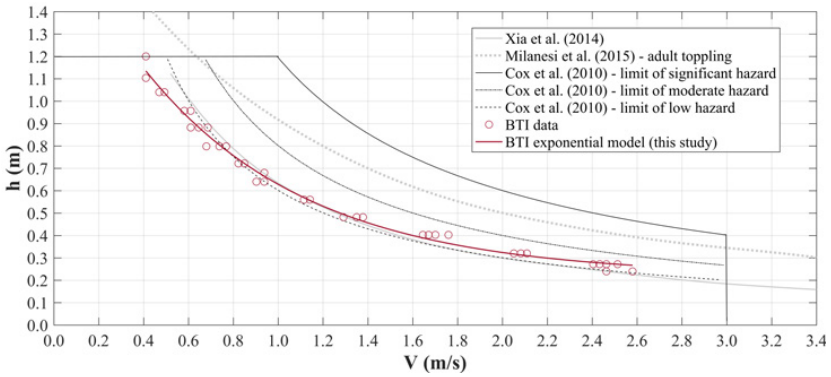

Figure 7: Experimental data (circles) and exponential regression model (red line) for BTI in comparison to the literature works (black and gray lines). The regression curve is represented within the experimental range. Prototype scale.

Finally, the joint analysis of R^2 and $\overline{SC}$ values, as reported in Table 5, suggests use of the exponential model to represent the data within the experimental range, as well as the limitation at $V = 3m/s$ to include sliding effects, from a conservative point of view.

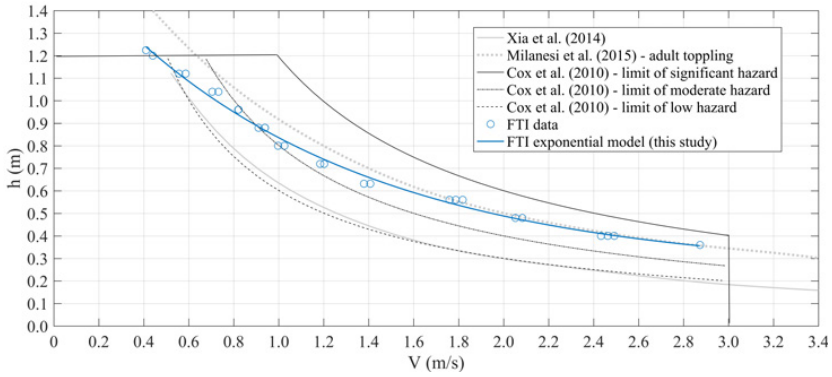

Figure 8: Experimental data (circles) and exponential regression model (blue line) for FTI in comparison to the literature works (black and gray lines). The regression curve is represented within the experimental range. Prototype scale.

3.3. Hydraulic forces and moments

The use of the theoretical approach for the static contributions leads to the estimate of F_{st} and M_{st} over the complete $h-V$ range, as illustrated in Figure 9a and b, respectively. Such panels illustrate constant values of F_{st} and M_{st} at a specific h value, i.e. constant with V and increasing with h.

The dynamic contributions have been estimated using the sensor measurements collected during the trolley in motion with constant speed V (for details, see Postacchini et al., 2019). Figure 9c and d show the additional dynamic force and moment, respectively. Both trends suggest a main dependence on the speed, i.e. both F_{dyn} and M_{dyn} do not change significantly with h but increase with V, although the maximum dynamic values are one order of magnitude smaller than the relative maximum static contributions. However, it is worth noting that the largest dynamic values occur in the lowermost part of the critical BTI and FTI curves (shown in red and blue, respectively, for convenience), where static and dynamic values are comparable.

The total force F_{tot} and moment M_{tot} are illustrated in Figure 9e and f, respectively. Here, the interplay between static and dynamic contributions is fairly evident, with the largest values not only concentrated in the upper part, but suggesting a trend, i.e. F_{tot} and M_{tot} reduce with both h and V, which resembles that of the BTI curve.

3.4. Dimensionless mobility

Figure 10 illustrates the collected data used to obtain the regression curve (section 3.2) plotted in a dimensionless fashion, using the parameters Fr, $\overline{h}$ and θ_P (section 2.5). The data distribution is compared to the theoretical curves introduced by Arrighi et al. (2019) and Arrighi et al. (2017), for the analysis of the overall human stability in floodwater conditions (Figure 10a and b, respectively).

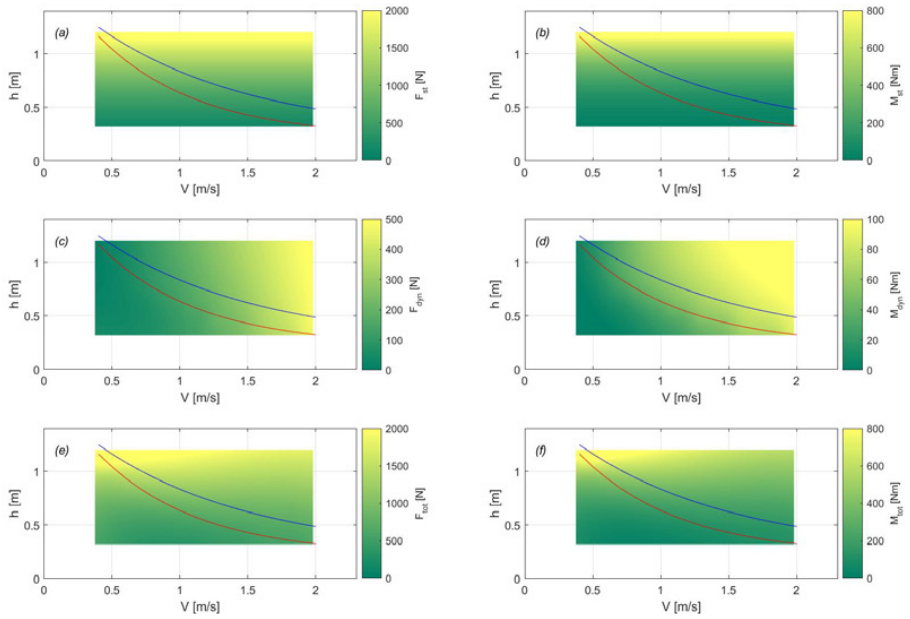

Figure 9: Exponential regression model for BTI (red lines) and FTI (blue lines) overlapped to color maps showing hydraulic forces (left panels) and moments (right panels): (a-b) hydrostatic contributions, (c-d) hydrodynamic contributions, (e-f) total.

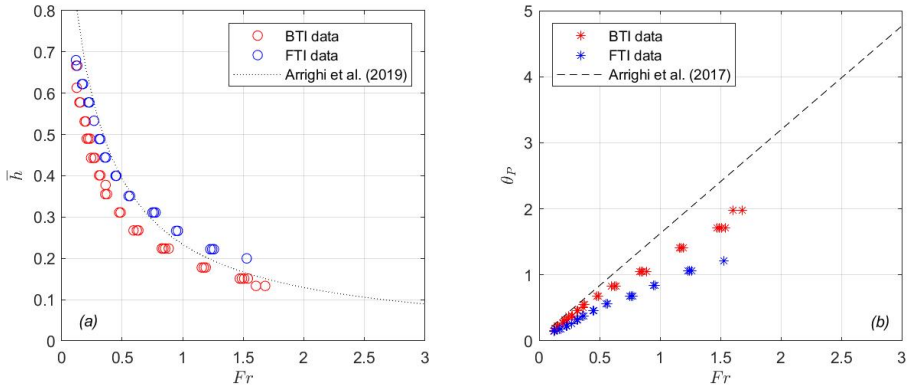

Figure 10: Distribution of critical BTI (red symbols) and FTI (blue symbols) values compared to theoretical curves (black lines): *(a)* $Fr - \overline{h}$ plane, *(b)* $Fr - \theta_P$ plane. Prototype scale.

Both BTI and FTI data qualitatively well distribute close to Arrighi et al. (2019)'s curve (Figure 10a), similar to the data used for the regression the curve itself (check fig.2 of Arrighi et al., 2019). It is worth noting that the BTI data (red circles) are all below the curve (dotted line), this highlighting a more critical condition: a fixed flow condition (Fr) leads to a smaller value of the critical height ($\overline{h}$) with respect to that provided by the theoretical curve. This

happens throughout the curve, although a dominance of the sliding mechanism (not considered in our tests) on the toppling mechanism typically occurs at large Fr values (e.g., see Arrighi et al., 2017). Further, the series of FTI data (blue circles) intersects the curve, this suggesting that relatively strong flows, i.e. either supercritical ($Fr > 1$) or close to the critical condition ($Fr \cong 1$), lead to conditions safer than those predicted using the literature curve, which refers to the classical BTI mechanism. The comparison between BTI and FTI data plotted in dimensionless fashion is in agreement with the dimensional fashion illustrated in Figure 6, with the largest differences occurring for fast flows, i.e. at large V and Fr values.

On the other hand, the distributions of BTI and FTI data in Figure 10b are significantly different, especially when compared to Arrighi et al. (2017)'s curve (dashed line) in the $Fr - \theta_P$ plane. Since the data are all below the theoretical line, such line seems not to be suitable to represent the critical condition for the present experiments, in particular for the FTI series. Specifically, a specific critical θ_P value corresponds to a flow condition Fr in the FTI experiments which is much larger than those prescribed by the theoretical curve, e.g. $Fr \sim 0.2$ (FTI) instead of $Fr \sim 0.1$ (theory) when $\theta_P \sim 0.2$, or $Fr \sim 1.5$ (FTI) instead of $Fr \sim 0.7$ (theory) when $\theta_P \sim 1.2$.

4. Discussion

4.1. On sliding and toppling behaviors

The analysis of the measured hydraulic pressures on the dummy legs highlights that

1. during low-speed/deep-water conditions, the hydrostatic components of force and moment are significantly larger (about one order of magnitude) than the hydrodynamic components;
2. during high-speed/shallow-water conditions, the hydrostatic components of force and moment are comparable to the hydrodynamic components, due to a large water level increase during the fluid-dummy interaction.

Further, the analyzed experimental data and the regression models described in Section 3 evidence how the stability is affected by the toppling mechanism for relatively small V values, also outside of the experimental range. From this point of view, both exponential and polynomial models are characterized by a maximum limit for stability that is similar to that individuated by Milanesi et al. (2015) for adults. In details, percentage difference between the limits of these studies are lower than 10%, as shown by Table 6. As for Milanesi et al. (2015), the instability at $V = 0m/s$ is reached when h is sufficiently close to the body height. Such limit condition moves towards the individuals' buoyancy phenomena (Cox et al., 2010; Bernardini et al., 2020), since here the hydrostatic contributions F_{st} and M_{st} are the main drivers for the final result, as shown by Figure 9a. From this point of view, according to Table 6, the logarithmic-based and the power-based models should be limited by a maximum value of h,

e.g. $1.2m$, as in all Cox et al. (2010)'s curves, since they cannot represent the buoyancy limitation from a theoretical viewpoint. According to a precautionary approach, it could be possible to limit all models to such value.

Meanwhile, the lower part of the curve (smaller depths and larger speeds) is dominated by the sliding mechanism, as confirmed by previous literature works (e.g., Cox et al., 2010). In such condition, both hydrodynamics forces F_{dyn} and moments M_{dyn} are the main drivers for the individuals' instability, as shown by Figure 9b. According to Table 6, both logarithmic and polynomial models confirm that instability conditions for sliding in terms of V proposed by previous works ($V \cong 3m/s$) exist (Cox et al., 2010), especially for BTI conditions. Capping the maximum speed for body stability at $3m/s$ as in Cox et al. (2010), regardless of h, allows to adopt a conservative approach to the sliding effects, especially in FTI conditions (here, $V > 4m/s$ for $h = 0m$ induces to sliding effects according to both models). On the contrary, both exponential and power laws should include a limitation in the maximum V values, since their theoretical formulation establishes a horizontal asymptotic trend for $V \to +\infty$, thus limiting the impact of sliding influence.

4.2. On behavioral implications for simulation and evaluation of risk reduction strategy

Although results are mainly referred to the tested $h - V$ pairs, i.e. $V \sim (0.4 - 3.0)m/s$ and $h \sim (0.2 - 1.2)m$, interesting remarks on the proposed modeling approaches can be provided to evidence further implications for the flood evacuation modeling issues, the risk assessment in urban areas and the proposal of risk-mitigation strategies. For the first time, BTI and FTI conditions for human body stability are assessed through a quasi-natural scale model using extensive laboratory tests. This result allows overcoming the limitation of current literature works, by highlighting the differences in human body stability due to the reciprocal position between individuals' body orientation and floodwater direction. Further, when the collected data are analyzed using dimensionless parameters, the existing theories based on both physical approaches and existing literature data (Arrighi et al., 2017, 2019) describe relatively well the BTI behavior, while the FTI data follow different trends and generally lead to safer conditions.

Hence, the dimensional BTI and FTI curves should be both included in simulation models based on microscopic approaches (Matsuo et al., 2011; Bernardini et al., 2017), by providing the evaluation of the body-floodwater direction versor as the main decisional task for the final stability of each simulated evacuee, in combination with the local floodwater features conditions (Cox et al., 2010; Milanesi et al., 2015; Bernardini et al., 2020). According to experimental results, the authors propose the use of the following equations 5 and 6 to calculate the limit for body stability in BTI and FTI conditions, respectively. A conservative approach for the body stability, based on the integration of results from previous works (Cox et al., 2010), is used to avoid the uncertainties due to the extension

of the results to $h - V$ pairs that are out of the experimental range:

$$\text{BTI stability if } \begin{cases} h \leq 1.2m & \text{for } V < 0.37m/s \\ h \leq \left(1.63\ e^{-1.37\ V} + 0.22\right) m & \text{for } V = (0.37 \div 3.00)\, m/s \end{cases} \quad (5)$$

$$\text{FTI stability if } \begin{cases} h \leq 1.2m & \text{for } V < 0.45m/s \\ h \leq \left(1.43\ e^{-0.88\ V} + 0.24\right) m & \text{for } V = (0.45 \div 3.00)\, m/s \end{cases} \quad (6)$$

It is worthy of notice that the BTI conditions seem to be about 34% more critical than the FTI conditions, according to the DAUC calculation between the exponential model curves. In FTI, the individual might try to move his/her barycenter against the flood to improve his/her stability (Jonkman and Penning-Rowsell, 2008). Hence, physical support for human body stability is more important while the evacuees are moving in the same direction and sense of the floodwaters. To this end, handrails can be integrated in the urban furniture so as to allow people to hang on them while evacuating (Bernardini et al., 2017). Meanwhile, it is important to use evacuation simulators to retrieve the probable motion direction of the evacuees in complex urban areas, by jointly considering the spontaneous evacuation behaviors, as well as the positioning of gathering areas. From this point of view, the integration of both equations 5 and 6 inside the simulators is a fundamental step.

Finally, the understanding of hydraulic forces and moments in the experimental tests provides a hint to better understand the flow dynamics which characterize the evacuation process, especially around critical conditions. Specifically, attention should be paid to relatively high-speed conditions, since an increase of the speed provides an increase of the water surface level (as already shown in Postacchini et al., 2019), i.e. the hydrodynamic contribution increases with the speed. Hence, larger speeds mean water-level increase, as well as larger hydraulic forces and moments on the dummy, which lead to a reduced human stability.

Nevertheless, further studies will be aimed at directly connect the human body stability with the floodwater force trends to consider the possibility of a multi-variables stability equation which can include additional forces due to local turbulence of waters, as well as the effect of additional instability-related forces, e.g. effects of sediment transport and debris flows (e.g., Melo et al., 2020).

5. Conclusions

The present work aims at carefully investigate the critical conditions which are at the basis of the human stability in floodwater conditions. Experimental tests have been carried out using a physical model at quasi-natural scale, based on scientific anthropometric analysis and on a novel non-inertial approach, where the flood is reconstructed through a dummy traveling within the water at rest. Test series aiming at investigating the human stability were carried out either with the model facing the flow or with its back toward the flow, the former

leading to a backward toppling, the latter to a forward toppling. The results confirmed a large difference between the two experimental configurations, despite existing literature stated an overall similarity. A detailed regression analysis, performed through comparison with literature curves, underlined the suitability of an exponential law for the interpolation of the experimental data and the description of the critical/stability curves related to both tested configurations.

A further analysis on the involved pressures highlight that deep waters and low flows correspond to a dominance of the hydrostatic components, while shallow waters and high flows lead to an interplay between hydrostatic and hydrodynamic components. In the latter case, the sliding mechanism is definitely prevailing on the toppling, due to large drag force generated by the high-speed flow, which strongly contrasts the stabilizing force provided by the friction between bottom and feet.

The proposed criteria for human stability representation should be implemented in evacuation simulators. In this sense, simulation models based on a microscopic approach will take advantage of this work results, since it will be possible to overlay the stability rules to the other motion behaviors assigned to each simulated individual. Effects of the relative evacuee-flow direction could be solved by adopting the two instability curves referred to forward and backward toppling conditions, thus providing specific safety levels according to the local floodwater characterization. The same model could be adopted in the simulation of the evacuation in complex outdoor and indoor environments (e.g. underground spaces), since similar evacuation risks can occur due to interactions between floodwaters, human motion and space layout.

The combination of the present results with evacuation speed representation and additional specific human choices in emergency conditions (such as safe area selection, interactions with obstacles, interactions with other individuals) will enable one to use flood evacuation simulators to:

a) effectively evaluate the risk conditions for the exposed pedestrians in the flood-affected environment;
b) verify where critical evacuation situations can occur due to floodwater-people interactions (i.e. stability loss);
c) provide (and evaluate) risk reduction strategies to reduce the impact of such situations, such as, in outdoor spaces, those related to: placing and dimensioning of raised platforms or sidewalks in urban areas to reduce instability issues and create areas where to wait for rescuers' support; placing of handrails or street furniture to guarantee support to evacuees; definition of evacuation paths and assembly areas taking into account both evacuee's and floodwater motion directions.

Acknowledgements

This work is fully supported by the scientific project "Building Resilience to flood Impact Deriving from Global warming in Europe (BRIDGE)" funded by Università Politecnica delle Marche, internal program 2017/2018. Dr. Fiorenza

Finizio, Dr. Beatrice Ascenzi, Dr. Ramona Bruni, Dr. Giuseppe Di Giovine and Mr. Livio Luccarini collaborated in the laboratory experiments and are strongly acknowledged.

References

Abt, S., Wittier, R., Taylor, A., Love, D.. Human stability in a high flood hazard zone 1. JAWRA Journal of the American Water Resources Association 1989;25(4):881–890.

Arrighi, C., Oumeraci, H., Castelli, F.. Hydrodynamics of pedestrians' instability in floodwaters. Hydrology and Earth System Sciences 2017;21(1):515–531.

Arrighi, C., Pregnolato, M., Dawson, R., Castelli, F.. Preparedness against mobility disruption by floods. Science of the Total Environment 2019;654:1010–1022.

Baba, Y., Ishigaki, T., Toda, K.. Experimental studies on safety evacuation from underground spaces under inundated situations. Journal of JSCE 2017;5(1):269–278.

Bernardini, G., Postacchini, M., Quagliarini, E., Brocchini, M., Cianca, C., D'Orazio, M.. A preliminary combined simulation tool for the risk assessment of pedestrians flood-induced evacuation. Environmental Modelling & Software 2017;96:14–29.

Bernardini, G., Quagliarini, E., D'Orazio, M., Brocchini, M.. Towards the simulation of flood evacuation in urban scenarios: Experiments to estimate human motion speed in floodwaters. Safety Science 2020;123:104563.

Brown, A.E., Zhang, L., McMahon, T.A., Western, A.W., Vertessy, R.A.. A review of paired catchment studies for determining changes in water yield resulting from alterations in vegetation. Journal of hydrology 2005;310(1-4):28–61.

Brown, R., Chanson, H.. Turbulence and suspended sediment measurements in an urban environment during the brisbane river flood of january 2011. Journal of Hydraulic Engineering 2012;139(2):244–253.

Chanson, H., Brown, R., McIntosh, D., et al. Human body stability in floodwaters: the 2011 flood in brisbane cbd. In: 11th National Conference on Hydraulics in Civil Engineering & 5th International Symposium on Hydraulic Structures: Hydraulic Structures and Society-Engineering Challenges and Extremes. Engineers Australia; 2014. p. 294.

Cox, R., Shand, T., Blacka, M.. Australian Rainfall and Runoff revision project 10: appropriate safety criteria for people. Technical Report; 2010.

CRED, . The human cost of weather-related disasters, 1995–2015. United Nations, Geneva 2015;.

Darvini, G., Memmola, F.. Assessment of the impact of climate variability and human activities on the runoff in five catchments of the adriatic coast of south-central italy. Journal of Hydrology: Regional Studies 2020;31:100712.

Dottori, F., Di Baldassarre, G., Todini, E.. Detailed data is welcome, but with a pinch of salt: Accuracy, precision, and uncertainty in flood inundation modeling. Water Resources Research 2013;49(9):6079–6085.

Fang, Q.. Adapting chinese cities to climate change. Science 2016;354(6311):425–426.

Foster, D.N., Cox, R.. Stability of Children on Roads Used as Floodways: Preliminary Study. Technical Report; 1973.

Heller, V.. Scale effects in physical hydraulic engineering models. Journal of Hydraulic Research 2011;49(3):293–306.

Herman, I.P.. Physics of the human body: Biological and medical physics. Biomedical Engineering Springer, Heidelberg 2016;.

Huntington, T.G.. Evidence for intensification of the global water cycle: review and synthesis. Journal of Hydrology 2006;319(1):83–95.

Jonkman, S., Penning-Rowsell, E.. Human instability in flood flows. JAWRA Journal of the American Water Resources Association 2008;44(5):1208–1218.

Kim, K., Pant, P., Yamashita, E.. Integrating travel demand modeling and flood hazard risk analysis for evacuation and sheltering. International journal of disaster risk reduction 2018;31:1177–1186.

Kundzewicz, Z.W., Kanae, S., Seneviratne, S.I., Handmer, J., Nicholls, N., Peduzzi, P., Mechler, R., Bouwer, L.M., Arnell, N., Mach, K., et al. Flood risk and climate change: global and regional perspectives. Hydrological Sciences Journal 2014;59(1):1–28.

Lind, N., Hartford, D., Assaf, H.. Hydrodynamic models of human stability in a flood. JAWRA Journal of the American Water Resources Association 2004;8:89–96.

Ma, Z., Kang, S., Zhang, L., Tong, L., Su, X.. Analysis of impacts of climate variability and human activity on streamflow for a river basin in arid region of northwest china. Journal of Hydrology 2008;352(3-4):239–249.

Matsuo, K., Natainia, L., Yamada, F.. Flood and evacuation simulations for urban flooding. In: 5th international conference on flood management. 2011. p. 391–398.

Melo, R., Zêzere, J., Oliveira, S., Garcia, R.A., Oliveira, S., Pereira, S., Piedade, A., Santos, P.P., van Asch, T.. Defining evacuation travel times and safety areas in a debris flow hazard scenario. Science of the total environment 2020;712:136452.

Memmola, F., Darvini, G.. Changes in precipitation-runoff relationship in six catchments of the adriatic coast of center italy. In: Proceedings of 13th International Conference on Hydroinformatics. 2018. .

Mignot, E., Li, X., Dewals, B.. Experimental modelling of urban flooding: A review. Journal of Hydrology 2019;568:334–342.

Milanesi, L., Pilotti, M., Ranzi, R.. A conceptual model of people's vulnerability to floods. Water Resources Research 2015;51(1):182–197.

Mollah, A.K., Sadhukhan, S., Das, P., Anis, M.Z.. A cost optimization model and solutions for shelter allocation and relief distribution in flood scenario. International Journal of Disaster Risk Reduction 2018;31:1187–1198.

Pachauri, R.K., Allen, M.R., Barros, V.R., Broome, J., Cramer, W., Christ, R., Church, J.A., Clarke, L., Dahe, Q., Dasgupta, P., et al. Climate change 2014: synthesis report. Contribution of Working Groups I, II and III to the fifth assessment report of the Intergovernmental Panel on Climate Change. IPCC, 2014.

Postacchini, M., Zitti, G., Giordano, E., Clementi, F., Darvini, G., Lenci, S.. Flood impact on masonry buildings: The effect of flow characteristics and incidence angle. Journal of Fluids and Structures 2019;88:48–70.

Ronchi, E., Kuligowski, E.D., Reneke, P.A., Peacock, R.D., Nilsson, D.. The process of verification and validation of building fire evacuation models. US Department of Commerce, National Institute of Standards and Technology , 2013.

Shand, T., Smith, G., Cox, R., Blacka, M., et al. Development of appropriate criteria for the safety and stability of persons and vehicles in floods. In: Proceedings of the 34th World Congress of the International Association for Hydro-Environment Research and Engineering: 33rd Hydrology and Water Resources Symposium and 10th Conference on Hydraulics in Water Engineering. Engineers Australia; 2011. p. 404.

Soldini, L., Darvini, G.. Extreme rainfall statistics in the marche region, italy. Hydrology Research 2017;48(3):686–700.

Wang, W., Shao, Q., Yang, T., Peng, S., Xing, W., Sun, F., Luo, Y.. Quantitative assessment of the impact of climate variability and human activities on runoff changes: a case study in four catchments of the haihe river basin, china. Hydrological Processes 2013;27(8):1158–1174.

Webb Associates, . Anthropometric source book - Volume III. volume 2. National Aeronautics and Space Administration, Scientific and Technical Information Office, 1978.

Xia, J., Falconer, R.A., Wang, Y., Xiao, X.. New criterion for the stability of a human body in floodwaters. Journal of Hydraulic Research 2014;52(1):93–104.

Zhang, L., Dawes, W., Walker, G.. Response of mean annual evapotranspiration to vegetation changes at catchment scale. Water resources research 2001;37(3):701–708.

Appendix A

The present section illustrates both abbreviations (Table 7) and symbols (Table 8) used in the manuscript.

Table 7: List of abbreviations.

Abbreviation	Description
BTI	Backward Toppling Instability
DAUC	Difference between the graphic Areas Under the Curves
FTI	Forward Toppling Instability
SC	Secant Cosine
EPC	Euclidean Projection Coefficient

Table 8: List of symbols.

Symbol	Description
a, b, c	fitting coefficients
D	cylinder diameter in the dummy concept
d_f	foot length
D_M	model diameter
F_{st}	hydrostatic force
F_{dyn}	hydrodynamic force
F_{tot}	total force
Fr	Froude number
g	gravity acceleration
h	water depth
$\overline{h}$	relative height
h_{exp}	water-depth estimation from regression models
h_{ref}	water depth from reference studies
H	height in the dummy concept
H_M	model height
H_P	prototype height
m_M	model mass
m_P	prototype mass
p_{st}	hydrostatic pressure at the bottom
p_d	hydrodynamic pressure
M_{st}	hydrostatic moment
M_{dyn}	hydrodynamic moment
M_{tot}	total moment
R^2	coefficient of determination
V	speed
V_M	model volume
$(x_c,\, y_c)$	mass coordinates in the dummy concept
γ	unit weight
θ_P	mobility parameter
λ_F	force scale
λ_l	length scale
λ_m	mass scale
λ_p	pressure scale
λ_v	velocity scale
λ_V	volume scale
ρ_M	model density